

**High-pressure and high-temperature single-crystal elasticity of Cr-pyrope:
implications for the density and seismic velocity of subcontinental lithospheric
mantle**

Jingui Xu^{1, 2}, Dawei Fan^{1*}, Bo Li³, Sergey N. Tkachev⁴, Vitali B. Prakapenka⁴,
Dongzhou Zhang², Guangzhong Yang⁵, Yi Zhou⁶, and Wenge Zhou¹

¹Key Laboratory for High-Temperature and High-Pressure Study of the Earth's Interior, Institute of Geochemistry, Chinese Academy of Sciences, Guiyang, Guizhou 550081, China.

² Hawai'i Institute of Geophysics and Planetology, School of Ocean and Earth Science and Technology, University of Hawai'i at Manoa, Honolulu, Hawaii 96822, United States.

³ Research Institute of Petroleum Exploration & Development-Northwest (NWGI), PetroChina, Lanzhou, 730060 China

⁴ Center for Advanced Radiation Sources, University of Chicago, Chicago, Illinois 60437, United States.

⁵ The No. 101 Geological Brigade, Geological and Mineral Exploration and Development Bureau of Guizhou Province, Kaili, Guizhou 556000, China.

⁶ School of Geoscience and Technology, Southwest Petroleum University, Chengdu, Sichuan 610500, China

*Corresponding authors: Dawei Fan (fandawei@mail.gyig.ac.cn)

Contents of this file

Texts S(1-2)

Figures S(1-5)

Tables S(1-6)

Text S1

The used third-order Birch-Murnaghan equation of state is described in the following:

$$P = \frac{3K_{T0}}{2} \left[\left(\frac{V_{T0}}{V} \right)^{\frac{7}{3}} - \left(\frac{V_{T0}}{V} \right)^{\frac{5}{3}} \right] \left\{ 1 + \frac{3}{4} \left((\partial K_T / \partial P)_T - 4 \right) \left[\left(\frac{V_{T0}}{V} \right)^{\frac{2}{3}} - 1 \right] \right\} \quad (1),$$

where P , V_{T0} , V , K_{T0} , and $(\partial K_T / \partial P)_T$ are pressure, unit-cell volume at temperature and zero-pressure, unit-cell volume at pressure and temperature, zero-pressure bulk modulus, and its pressure derivative, respectively.

The thermal-pressure equation of state is based on the idea of thermal pressure (P_{th} ; e.g., (Angel et al., 2014). The total pressure (P) at a given V and T can be expressed as $P(V, T) = P(V, T_{ref}) + P_{th}$. $P(V, T_{ref})$ is the pressure at reference temperature (T_{ref}) which is described by the Birch-Murnaghan equation of state (1). P_{th} used here is proposed by Holland & Powell (2011):

$$P_{th} = \alpha_0 K_{T0} \left(\frac{\theta_E}{\zeta_0} \right) \left(\frac{1}{\exp(\theta_E/T) - 1} - \frac{1}{\exp(\theta_E/T_{ref}) - 1} \right) \quad (2),$$

where α_0 is the thermal expansion coefficient at T_{ref} , θ_E is the Einstein temperature, and ζ_0 is given by the following expression (Kroll et al., 2012):

$$\zeta_0 = \frac{(\theta_E/T_{ref})^2 \exp(\theta_E/T_{ref})}{(\exp(\theta_E/T_{ref}) - 1)^2} \quad (3).$$

Text S2

The adiabatic bulk (K_S) and shear (G) modulus at high P and high T are evaluated by the third- or fourth-order finite-strain equations.

(1) For K_S :

$$K_S = K_{S0}(T) \times (1 + 2f)^{\left(\frac{5}{2}\right)} \times \left(1 + \left(3 \left(\frac{\partial K_S}{\partial P} \right)_T - 5 \right) \times f \right) \text{ or}$$

$$K_S = K_{S0}(T) \times (1 + 2f)^{\left(\frac{5}{2}\right)} \times \left(1 + \left(3 \left(\frac{\partial K_S}{\partial P} \right)_T - 5 \right) \times f + 0.5 \times \left(9K_{S0}(T) \times \left(\frac{\partial^2 K_S}{\partial P^2} \right)_T + 9 \times \left(\frac{\partial K_S}{\partial P} \right)_T^2 - 36 \times \left(\frac{\partial K_S}{\partial P} \right)_T + 35 \right) \times f^2 \right) \quad (4),$$

$$K_{S0}(T) = K_{S0} + \left(\frac{\partial K_S}{\partial T} \right)_P \times (T - T_{ref}) \quad (5),$$

$$\left(\frac{\partial K_S}{\partial P} \right)_T = \left(\frac{\partial K_S}{\partial P} \right)_{T_{ref}} \times \text{Exp} \int_{T_{ref}}^T \alpha \, dT \quad (6),$$

$$f = 0.5 \times \left(\left(\frac{\rho}{\rho_0(T)} \right)^{\frac{2}{3}} - 1 \right) \quad (7),$$

$$\rho_0(T) = \rho_0(T_{ref}) \times \left(\text{Exp} \int_{T_{ref}}^T \alpha \, dT \right)^{-1} \quad (8),$$

where $K_{S0}(T)$ is the adiabatic bulk modulus at room P and temperature (T) , f is the Eulerian finite strain, $\left(\frac{\partial K_S}{\partial P}\right)_T$ is the first-order pressure derivative of K_S at temperature T , $\left(\frac{\partial^2 K_S}{\partial P^2}\right)_T$ is the second-order pressure derivative of K_S at T , K_{S0} is the adiabatic bulk modulus at room P - T , $\left(\frac{\partial K_S}{\partial T}\right)_P$ is the temperature derivative of K_S , $\left(\frac{\partial K_S}{\partial P}\right)_{T_{ref}}$ is the first pressure derivative of K_S at T_{ref} , ρ is the density at high P - T , $\rho_0(T)$ is the density at room P and T , $\rho_0(T_{ref})$ is the density at room P - T , and α is the thermal expansion coefficient.

(2) For G

$$G = (1+2f)^{\frac{5}{2}} \times (G_0(T) + b_1 f) \text{ or}$$

$$G = (1 + 2f)^{\frac{5}{2}} \times (G_0(T) + b_1 f + 0.5b_2 f^2) \quad (9),$$

$$G_0(T) = G_0 + \left(\frac{\partial G}{\partial T}\right)_P \times (T - T_{ref}) \quad (10),$$

$$b_1 = 3K_{T0}(T) \left(\frac{\partial G}{\partial P}\right)_T - 5G_0(T) \quad (11),$$

$$b_2 = 9(K_{T0}^2(T) \left[\left(\frac{\partial^2 G}{\partial P^2}\right)_T + 1/K_{T0}(T) \left(\left(\frac{\partial K_T}{\partial P}\right)_T - 4\right) \left(\frac{\partial G}{\partial P}\right)_T\right] + \frac{35G_0(T)}{9}) \quad (12),$$

$$\left(\frac{\partial G}{\partial P}\right)_T = \left(\frac{\partial G}{\partial P}\right)_{T_{ref}} \times \text{Exp} \int_{T_{ref}}^T \alpha_0 dT \quad (13),$$

$$K_{T0} = K_{S0} / (1 + \alpha\gamma T) \quad (14),$$

$$\left(\frac{\partial K_T}{\partial P}\right)_T = (1 + \alpha\gamma T)^{-1} \times \left(\left(\frac{\partial K_S}{\partial P}\right)_T - \gamma T / K_{T0}(T) \left(\frac{\partial K_T}{\partial T}\right)_P \right) \quad (15),$$

$$\left(\frac{\partial K_T}{\partial T}\right)_P = \left(\frac{\partial K_S}{\partial T}\right)_P - \alpha\gamma T / (1 + \alpha\gamma T) \quad (16),$$

where $G_0(T)$ is the shear modulus at room P and temperature T , G_0 is the shear modulus at room P - T , $\left(\frac{\partial G}{\partial T}\right)_P$ is the temperature derivative of G , $K_{T0}(T)$ is the isothermal bulk modulus at room- P and T , $\left(\frac{\partial G}{\partial P}\right)_T$ is the first-order pressure derivative of G at T , $\left(\frac{\partial^2 G}{\partial P^2}\right)_T$ is the second-order pressure derivative of G , $\left(\frac{\partial K_T}{\partial P}\right)_T$ is the pressure derivative of the isothermal bulk modulus at T , $\left(\frac{\partial G}{\partial P}\right)_{T_{ref}}$ is the pressure derivative of G at T_{ref} , K_{T0} is the isothermal bulk modulus at room P - T , γ is the Grüneisen

parameter, $\left(\frac{\partial K_T}{\partial P}\right)_T$ is the pressure derivative of the isothermal bulk modulus at T , and

$\left(\frac{\partial K_T}{\partial T}\right)_P$ is the temperature derivative of the isothermal bulk modulus.

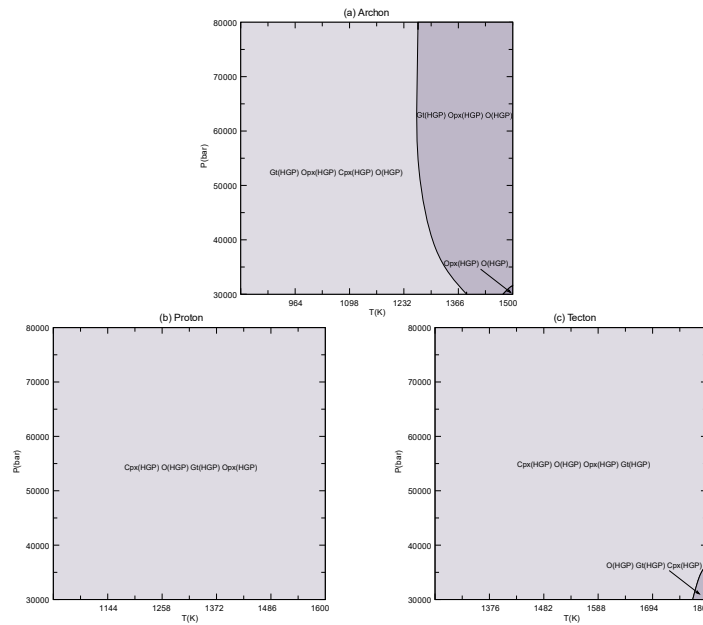


Figure S1. The calculated phase diagrams using *Perple_X* for the Archon (a), Proton (b), and Tecton (c) SCLM. O-olivine; Opx-orthopyroxene; Cpx-clinopyroxene; Gt-garnet. HGP means the used solution model.

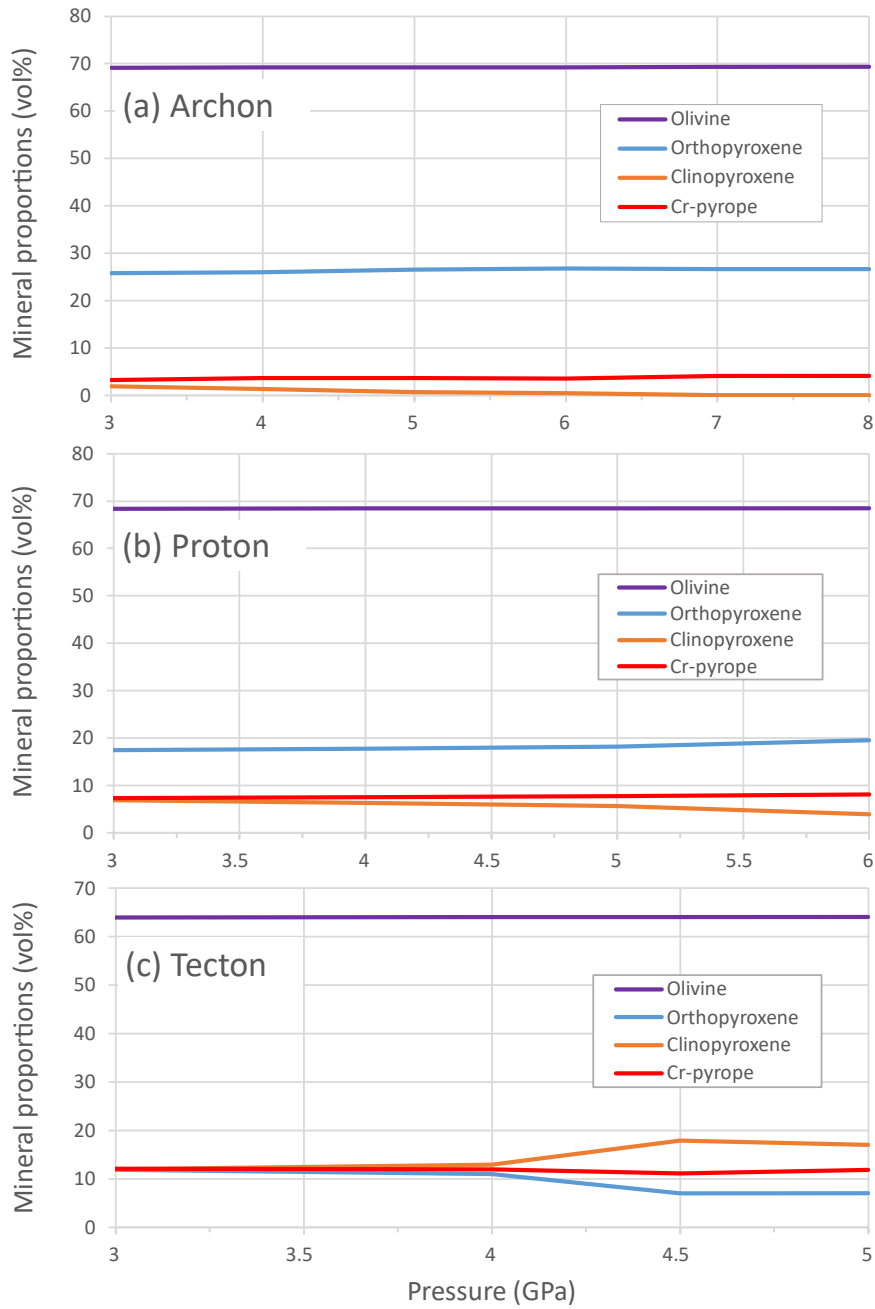


Figure S2. Calculated mineral proportions of three SCLMs, (a) Archon (3-8 GPa), (b) Proton (3-6 GPa), and (c) Tecton (3-5 GPa). The used bulk compositions of the SCLMs are extracted from Griffin et al. (2009), and the used geotherms are taken from Deen et al. (2006).

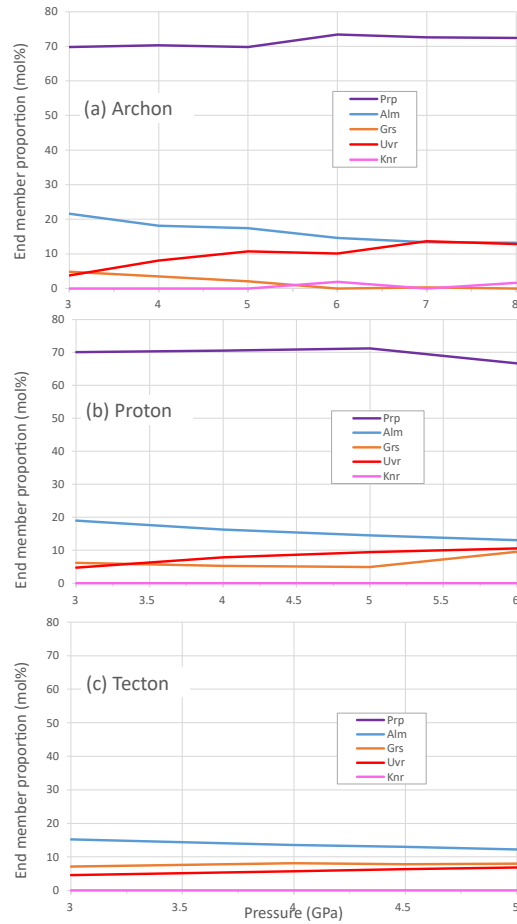


Figure S3. End-member proportions of Cr-pyrope in the Archon (a; 3-8 GPa), Proton (b; 3-6 GPa) and Tecton (c; 3-5 GPa). Prp, Alm, Grs, Uvr and Knr represent pyrope, almandine, grossular, uvarovite and knorringite, respectively.

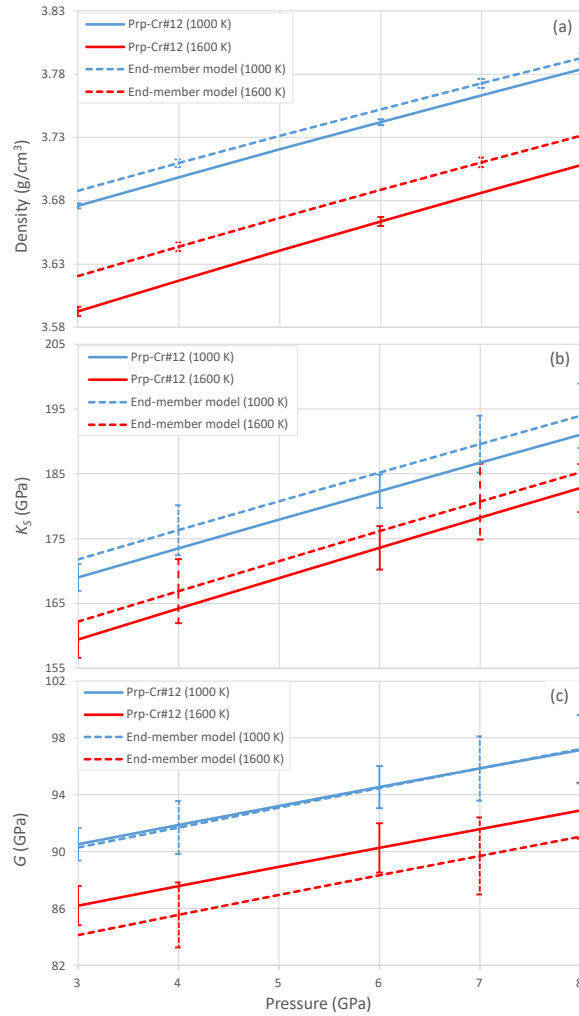


Figure S4. Density ρ (a), bulk modulus K_S (b) and shear modulus G (c) of Prp-Cr#12 along isotherms at 1000 K and 1600 K over 3–8 GPa. The solid curves represent values calculated using the elastic parameters (Table S3) fitted to the Prp-Cr#12 data. The dashed curves represent values calculated using the end-member model (linear average of garnet end-member parameters; Table S4) elastic parameters determined for the Prp-Cr#12 composition. Error bars are shown at selected pressures.

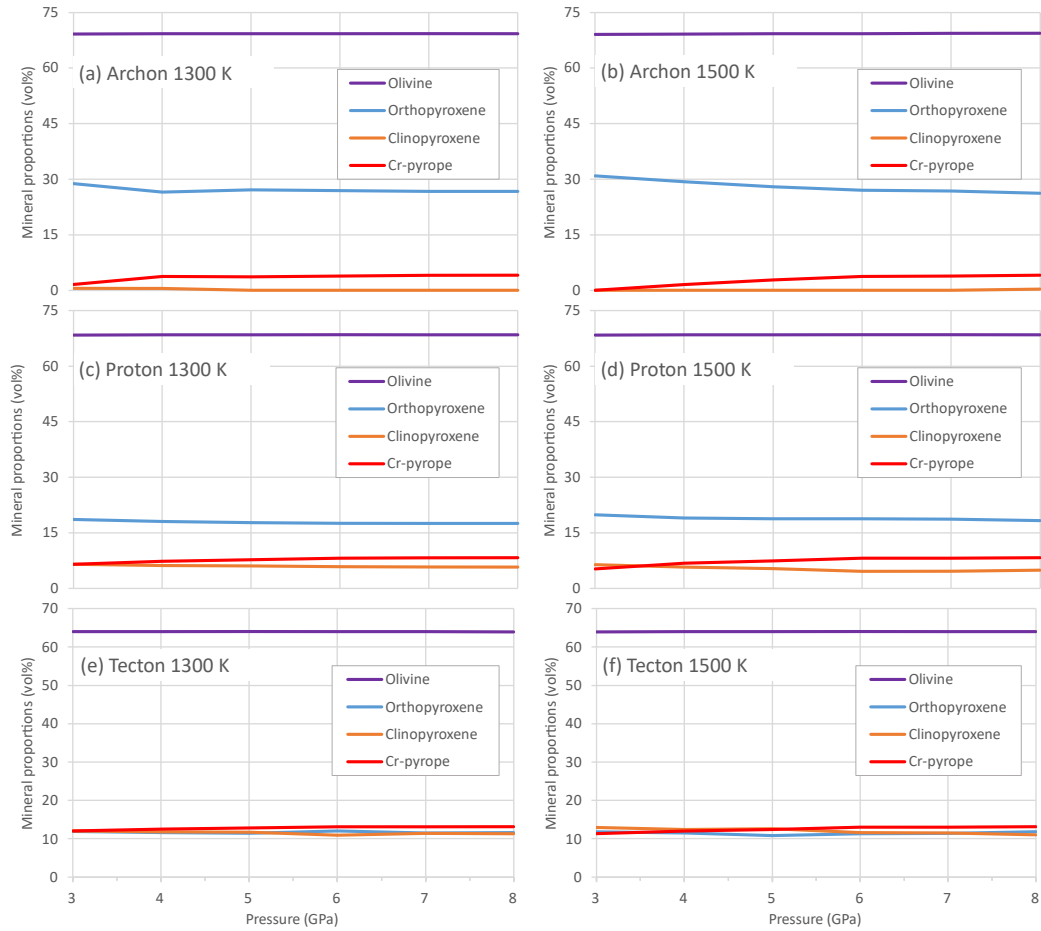


Figure S5. Calculated mineral proportions of three SCLMs, (a) Archon, (b) Proton, and (c) Tecton at 3-8 GPa along isotherms at 1300 K and 1500 K. The major-element compositions of the SCLMs are extracted from Griffin et al. (2009).

Table S1. Average compositions of the Archon, Proton, and Tecton SCLM adopted from Griffin et al. (2009), which are used for the Perple_X calculation

Oxide (wt.%)	Archon	Proton	Tecton
SiO ₂	45.7	44.7	44.5
Al ₂ O ₃	0.99	2.1	3.5
FeO	6.4	7.9	8.0
MgO	45.5	42.4	39.8
CaO	0.59	1.9	3.1
Na ₂ O	0.07	0.15	0.24
Cr ₂ O ₃	0.28	0.42	0.40

Note: other minor components (e.g., TiO₂, MnO) are not considered in the Perple_X calculation.

Table S2. Mineral proportions and compositions of the Archon (a), Proton (b) and Tecton (c) as a function of pressure and temperature

Pressure (GPa)	Temperature (K)	Ol/Opx/Cpx /Gt (vol. %)	Ol	Opx	Cpx	Gt				
(a) Archon										
3	835	69.1/25.8/1.9/3.2	Mg _{1.85} Fe _{0.15} SiO ₄ Fa _{7.25}	Fo _{92.75} Fa _{7.25}	Mg _{1.84} Fe _{0.12} Ca _{0.01} Na _{0.01} Cr _{0.02} Al _{0.02} Si _{1.98} O ₆	En _{90.71} Fs _{5.99} Di _{0.8} Kos _{0.8} Jd ₀ MgTs _{0.6} CrEn _{1.1}	Mg _{0.85} Fe _{0.03} Ca _{0.84} Na _{0.14} Cr _{0.08} Al _{0.06} Si ₂ O ₆	Di _{80.7} Jd ₆ Hd _{3.2} Cen _{1.9} Kos _{8.2} CaTs ₀	Mg _{2.09} Fe _{0.65} Ca _{0.26} Cr _{0.08} Al _{1.92} Si ₃ O ₁₂	Prp _{69.8} Alm _{21.6} Grs _{4.8} Uvr _{3.8} Knr ₀
4	987	69.2/26/1.3/3.6	Mg _{1.85} Fe _{0.15} Si _{1.99} O ₆ Fa _{7.40}	Fo _{92.60} Fa _{7.40}	Mg _{1.84} Fe _{0.11} Ca _{0.02} Na _{0.01} Cr _{0.01} Al _{0.02} Si _{1.99} O ₆	En _{90.51} Fs _{5.49} Di _{1.9} Kos _{1.1} Jd ₀ MgTs _{0.7} CrEn _{0.2}	Mg _{0.87} Fe _{0.03} Ca _{0.84} Na _{0.13} Cr _{0.07} Al _{0.06} Si ₂ O ₆	Di _{80.82} Jd _{5.59} Hd _{3.4} Cen ₃ Kos _{7.19} CaTs ₀	Mg _{2.11} Fe _{0.54} Ca _{0.35} Cr _{0.16} Al _{1.84} Si ₃ O ₁₂	Prp _{70.3} Alm _{18.1} Grs _{3.5} Uvr _{8.1} Knr ₀
5	1123	69.2/26.5/0.7/3.6	Mg _{1.85} Fe _{0.15} SiO ₄ Fa _{7.50}	Fo _{92.50} Fa _{7.50}	Mg _{1.83} Fe _{0.1} Ca _{0.03} Na _{0.02} Cr _{0.01} Al _{0.02} Si _{1.99} O ₆	En _{88.11} Fs _{4.8} Di _{4.5} Kos _{1.1} Jd _{0.5} MgTs ₁ CrEn ₀	Mg _{0.89} Fe _{0.03} Ca _{0.87} Na _{0.1} Cr _{0.06} Al _{0.04} Si ₂ O ₆	Di _{84.02} Jd _{4.4} Hd _{3.1} Cen _{2.6} Kos _{5.89} CaTs ₀	Mg _{2.1} Fe _{0.52} Ca _{0.38} Cr _{0.21} Al _{1.79} Si ₃ O ₁₂	Prp _{69.8} Alm _{17.4} Grs _{2.1} Uvr _{10.7} Knr ₀
6	1242	69.2/26.8/0.5/3.5	Mg _{1.85} Fe _{0.15} SiO ₄ Fa _{7.70}	Fo _{92.30} Fa _{7.70}	Mg _{1.82} Fe _{0.1} Ca _{0.05} Na _{0.02} Cr _{0.01} Al _{0.03} Si _{1.99} O ₆	En _{88.91} Fs _{4.6} Di _{4.7} Kos _{0.7} Jd _{1.1} MgTs ₀ CrEn ₀	Mg _{0.93} Fe _{0.04} Ca _{0.84} Na _{0.1} Cr _{0.06} Al _{0.04} Si ₂ O ₆	Di _{79.7} Jd _{4.2} Hd ₄ Cen _{6.5} Kos _{5.6} CaTs ₀	Mg _{2.26} Fe _{0.44} Ca _{0.3} Cr _{0.24} Al _{1.76} Si ₃ O ₁₂	Prp _{73.43} Alm _{14.59} Grs ₀ Uvr _{10.09} Knr _{1.9}
7	1345	69.3/26.7/0/4	Mg _{1.85} Fe _{0.15} SiO ₄ Fa _{7.75}	Fo _{92.25} Fa _{7.75}	Mg _{1.83} Fe _{0.09} Ca _{0.05} Na _{0.02} Cr _{0.01} Al _{0.01} Si ₂ O ₆	En _{88.91} Fs _{4.4} Di _{4.9} Kos _{0.5} Jd _{1.3} MgTs ₀ CrEn ₀	-	-	Mg _{2.18} Fe _{0.4} Ca _{0.42} Cr _{0.27} Al _{1.73} Si ₃ O ₁₂	Prp _{72.6} Alm _{13.4} Grs _{0.3} Uvr _{13.7} Knr ₀
8	1431	69.3/26.7/0/4.1	Mg _{1.84} Fe _{0.16} SiO ₄ Fa _{7.80}	Fo _{92.20} Fa _{7.80}	Mg _{1.83} Fe _{0.09} Ca _{0.05} Na _{0.02} Cr _{0.01} Al _{0.01} Si ₂ O ₆	En _{89.2} Fs _{5.2} Di _{3.2} Kos _{1.2} Jd _{0.3} MgTs _{0.9} CrEn ₀	-	-	Mg _{2.22} Fe _{0.4} Ca _{0.38} Cr _{0.29} Al _{1.71} Si ₃ O ₁₂	Prp _{72.4} Alm _{13.2} Grs ₀ Uvr _{2.8} Knr _{1.6}
(b) Proton										
3	1032	68.4/17.4/6.9/7.3	Mg _{1.81} Fe _{0.19} SiO ₄ Fa _{9.3}	Fo _{90.7} Fa _{9.3}	Mg _{1.79} Fe _{0.14} Ca _{0.02} Na _{0.01} Cr _{0.02} Al _{0.04} Si _{1.97} O ₆	En ₈₇ Fs _{7.2} Di _{2.1} Kos _{1.1} Jd ₀ MgTs _{1.5} CrEn _{1.1}	Mg _{0.87} Fe _{0.05} Ca _{0.83} Na _{0.12} Cr _{0.06} Al _{0.06} Si ₂ O ₆	Di _{77.5} Jd _{6.3} Hd _{5.2} Cen _{4.9} Kos _{6.1} CaTs ₀	Mg _{2.1} Fe _{0.57} Ca _{0.33} Cr _{0.1} Al _{1.91} Si ₃ O ₁₂	Prp _{70.03} Alm _{18.98} Grs _{6.19} Uvr _{4.8} Knr ₀
4	1238	68.4/17.7/6.3/7.5	Mg _{1.81} Fe _{0.19} SiO ₄ Fa _{9.5}	Fo _{90.5} Fa _{9.5}	Mg _{1.77} Fe _{0.13} Ca _{0.04} Na _{0.02} Cr _{0.02} Al _{0.04} Si _{1.98} O ₆	En _{85.31} Fs _{6.69} Di _{4.3} Kos _{1.5} Jd _{0.2} MgTs ₂ CrEn ₀	Mg _{0.92} Fe _{0.06} Ca _{0.78} Na _{0.12} Cr _{0.04} Al _{0.08} Si ₂ O ₆	Di ₇₂ Jd _{7.7} Hd _{6.1} Cen ₁₀ Kos _{4.2} CaTs ₀	Mg _{2.12} Fe _{0.49} Ca _{0.4} Cr _{0.16} Al _{1.84} Si ₃ O ₁₂	Prp _{70.53} Alm _{16.28} Grs _{5.29} Uvr _{7.89} Knr ₀
5	1425	68.5/18.1/5.7/7.7	Mg _{1.81} Fe _{0.19} SiO ₄ Fa _{9.65}	Fo _{90.35} Fa _{9.65}	Mg _{1.75} Fe _{0.13} Ca _{0.07} Na _{0.02} Cr _{0.01} Al _{0.04} Si _{1.99} O ₆	En _{83.22} Fs _{6.29} Di _{6.79} Kos _{1.2} Jd _{1.1} MgTs _{1.4} CrEn ₀	Mg _{0.98} Fe _{0.07} Ca _{0.73} Na _{0.11} Cr _{0.03} Al _{0.08} Si ₂ O ₆	Di _{66.23} Jd _{7.89} Hd _{6.89} Cen _{15.68} Kos _{3.2} CaTs _{0.1}	Mg _{2.14} Fe _{0.43} Ca _{0.43} Cr _{0.19} Al _{1.81} Si ₃ O ₁₂	Prp _{71.2} Alm _{14.5} Grs _{4.9} Uvr _{9.4} Knr ₀
6	1592	68.5/19.5/3.9/8.1	Mg _{1.8} Fe _{0.2} SiO ₄ Fa _{9.76}	Fo _{90.24} Fa _{9.76}	Mg _{1.73} Fe _{0.11} Ca _{0.09} Na _{0.03} Cr _{0.01} Al _{0.03} Si ₂ O ₆	En _{81.42} Fs _{6.69} Di _{9.39} Kos _{0.8} Jd _{2.2} MgTs _{0.5} CrEn ₀	Mg _{1.03} Fe _{0.07} Ca _{0.67} Na _{0.12} Cr _{0.03} Al _{0.09} Si ₂ O ₆	Di _{60.14} Jd _{8.99} Hd _{7.09} Cen _{21.28} Kos _{2.5} CaTs ₀	Mg ₂ Fe _{0.39} Ca _{0.61} Cr _{0.21} Al _{1.79} Si ₃ O ₁₂	Prp _{66.7} Alm _{13.1} Grs _{9.6} Uvr _{10.6} Knr ₀
(c) Tecton										
3	1270	64.0/11.9/12.0/12.1	Mg _{1.8} Fe _{0.2} SiO ₄ Fa _{10.01}	Fo _{89.99} Fa _{10.01}	Mg _{1.74} Fe _{0.14} Ca _{0.05} Na _{0.02} Cr _{0.02} Al _{0.08} Si _{1.96} O ₆	En _{82.42} Fs _{7.19} Di _{4.9} Kos _{1.6} Jd ₀ MgTs _{3.7} CrEn _{0.2}	Mg _{0.93} Fe _{0.07} Ca _{0.76} Na _{0.13} Cr _{0.03} Al _{0.1} Si ₂ O ₆	Di _{69.23} Jd _{9.89} Hd _{6.49} Cen _{11.69} Kos _{2.7} CaTs ₀	Mg _{2.19} Fe _{0.46} Ca _{0.35} Cr _{0.09} Al _{1.91} Si ₃ O ₁₂	Prp _{73.1} Alm _{15.2} Grs _{7.1} Uvr _{4.6} Knr ₀
4	1538	64.0/11.0/13.0/12.0	Mg _{1.8} Fe _{0.2} SiO ₄ Fa _{10.11}	Fo _{89.89} Fa _{10.11}	Mg _{1.7} Fe _{0.14} Ca _{0.08} Na _{0.02} Cr _{0.01} Al _{0.09} Si _{1.96} O ₆	En _{78.7} Fs _{6.9} Di _{8.3} Kos _{1.2} Jd _{0.9} MgTs ₄ CrEn ₀	Mg _{1.05} Fe _{0.09} Ca _{0.63} Na _{0.11} Cr _{0.02} Al _{0.11} Si _{1.99} O ₆	Di _{52.8} Jd _{9.2} Hd _{9.1} Cen ₂₆ Kos ₂ CaTs _{0.9}	Mg _{2.18} Fe _{0.41} Ca _{0.41} Cr _{0.11} Al _{1.89} Si ₃ O ₁₂	Prp _{72.7} Alm _{13.5} Grs _{8.1} Uvr _{5.7} Knr ₀
4.5	1664	64.0/7.0/17.9/11.1	Mg _{1.8} Fe _{0.2} SiO ₄ Fa _{10.17}	Fo _{89.83} Fa _{10.17}	Mg _{1.71} Fe _{0.13} Ca _{0.09} Na _{0.03} Cr _{0.01} Al _{0.05} Si _{1.99} O ₆	En _{80.12} Fs _{6.39} Di _{9.39} Kos _{0.7} Jd _{2.1} MgTs _{1.3} CrEn ₀	Mg _{1.2} Fe _{0.11} Ca _{0.47} Na _{0.08} Cr _{0.02} Al _{0.17} Si _{1.95} O ₆	Di _{29.9} Jd _{6.5} Hd _{11.2} Cen _{45.3} Kos _{1.7} CaTs _{5.4}	Mg _{2.19} Fe _{0.39} Ca _{0.43} Cr _{0.13} Al _{1.87} Si ₃ O ₁₂	Prp _{72.83} Alm _{12.99} Grs _{7.79} Uvr _{6.39} Knr ₀
5	1787	64.1/7.0/17.1/11.9	Mg _{1.8} Fe _{0.2} SiO ₄ Fa _{10.23}	Fo _{89.77} Fa _{10.23}	Mg _{1.67} Fe _{0.13} Ca _{0.12} Na _{0.03} Cr _{0.01} Al _{0.08} Si _{1.97} O ₆	En _{75.62} Fs _{6.29} Di _{12.39} Kos _{0.8} Jd _{1.8} MgTs _{3.1} CrEn ₀	Mg _{1.24} Fe _{0.11} Ca _{0.45} Na _{0.09} Cr _{0.01} Al _{0.13} Si _{1.98} O ₆	Di _{31.8} Jd _{7.6} Hd ₁₁ Cen _{46.1} Kos ₁ CaTs _{2.4}	Mg _{2.19} Fe _{0.37} Ca _{0.44} Cr _{0.14} Al _{1.86} Si ₃ O ₁₂	Prp ₇₃ Alm _{12.2} Grs ₈ Uvr _{6.8} Knr ₀

Notes: Ol-olivine; Opx-orthopyroxene; Cpx-clinopyroxene; Gt-garnet; Fo-Forsterite (Mg₂SiO₄); Fa-fayalite (Fe₂SiO₄); En-enstatite (Mg₂Si₂O₆); Fs-Ferrosilite (Fe₂Si₂O₆); MgTs-Mg-tschermakite (MgAlSiAlO₆); Di-diopside (CaMgSi₂O₆); Jd-jadeite (NaAlSi₂O₆); Kos-kosmochlor (NaCrSi₂O₆); CrEn-Cr-enstatite (MgCrSiAlO₆); Hd-hedenbergite (CaFeSi₂O₆); Cen-clinoenstatite (Mg₂Si₂O₆); CaTs-Ca-tschermakite (CaAlSiAlO₆); Prp-pyrope (Mg₃Al₂Si₃O₁₂); Alm-Almandine (Fe₃Al₂Si₃O₁₂); Grs-grossular (Ca₃Al₂Si₃O₁₂); Uvr-uvarovite (Ca₃Cr₂Si₃O₁₂); Knr-knorringite (Mg₃Cr₂Si₃O₁₂). - means unavailable. The geotherms of Archon, Proton, and Tecton are adopted from Deen et al. (2006)

Table S3. Chemical Composition of the Cr-pyrope in this study

Oxide (wt.%)	Prp-Cr#12
SiO ₂	41.77(58)
TiO ₂	0.09(3)
Al ₂ O ₃	19.91(23)
FeO ^a	6.39(4)
MnO	0.33(3)
MgO	20.15(24)
CaO	6.18(4)
Na ₂ O	0.01(1)
K ₂ O	0.00(0)
Cr ₂ O ₃	4.33(6)
NiO	0.01(2)
Total	99.20(100)

Numbers in parenthesis represent standard deviations

^a All Fe as FeO

Table S4. Elastic properties of Cr-pyrope and end-member pyrope

Composition	C_{11} (GPa)	C_{12} (GPa)	C_{44} (GPa)	K_{S0} (GPa)	G_0 (GPa)	V_P (km/s)	V_S (km/s)	$(\partial K_S/\partial P)_T$	$(\partial G/\partial P)_T$	$(\partial K_S/\partial T)_P$ (GPa/K)	$(\partial G/\partial T)_P$ (GPa/K)	Method	References
Cr-Prp ^a	291.4(6)	105.9(4)	90.6(3)	167.7(8)	91.5(5)	8.85(1)	4.97(1)	4.3(1)	1.4(1)	-0.0175(1)	-0.0073(1)		This study
Cr-Prp ^b	-	-	-	171.6(13)	90.7(1)	8.92(3)	4.99(1)	-	-	-	-	RPR	Babuška et al. (1978)
Cr-Prp ^c	-	-	-	171.3(16)	92.6(2)	8.92(4)	5.00(1)	-	-	-	-		
Cr-Prp ^d	-	-	-	170.0(18)	92.6(1)	8.90(5)	5.00(1)	-	-	-	-		
Cr-Prp ^e	-	-	-	170.8(27)	92.0(2)	8.88(7)	4.97(1)	-	-	-	-		
Cr-Prp ^f	296.6(15)	108.5(16)	91.6(2)	171.2(8)	92.6(3)	8.92	5.00			-0.0193(2) ^g	-0.0102(1) ^g	RPR	Suzuki & Anderson (1983)
Prp ₁₀₀ ^h	294.5(5)	105.7(6)	90.5(4)	168.6(4)	92.0(3)	9.05(1)	5.09(1)	4.6(1)	1.3(1)	-0.015(1)	-0.008(1)	BLS	Fan et al. (2019)
Prp ₁₀₀ ^h	296.2(5)	111.1(6)	91.6(3)	172.8(3)	92.0(2)	9.06	5.11	-	-	-	-	BLS	O'Neill et al. (1991)
Prp ₁₀₀	295(2)	117(1)	90(3)	177(1)	89(1)	9.08	5.10	-	-	-	-	BLS	Leitner et al. (1980)
Prp ₁₀₀	297(3)	108(2)	93(2)	171(2)	94(2)	9.115	5.125	4.1(3)	1.3(2)	-	-	BLS	Sinogeikin & Bass (2000)
Prp ₁₀₀	298(3)	107(2)	93(2)	171(2)	94(2)	-	-	-	-	-0.014(2)	-0.009(1)	BLS	Sinogeikin & Bass (2002)
Prp ₁₀₀	-	-	-	170(2)	93(1)	9.10(5)	5.12(3)	4.3(3)	1.5(2)	-	-	UI	Gwanmesia et al. (2006)
Prp ₁₀₀	-	-	-	166.0(2)	92.2(1)	9.01	5.09	-	-	-0.0193(4)	-0.0104(2)	UI	Gwanmesia et al. (2007)
Prp ₁₀₀	-	-	-	171(2)	92(1)	9.07(5)	5.07(3)	5.3(4)	1.6(2)	-	-	UI	Chen et al. (1999)
Prp ₁₀₀	-	-	-	172.0(16)	89.1(5)	-	-	4.38(8)	1.66(5)	-0.018(2)	-0.008(1)	UI	Chantel et al. (2016)
Prp ₁₀₀	-	-	-	170.0(2)	93.2(1)	-	-	4.51(2)	1.51(2)	-0.0170(1)	-0.0107(1)	UI	Zou, Irifune, et al. (2012)

Notes:^a Prp_{71.0}Alm_{12.6}Sps_{0.7}Grs_{3.5}Uvr_{12.2},^b Prp_{73.1}Alm_{14.3}Adr_{3.1}Sps_{0.6}Uvr_{8.9},^c Prp_{72.6}Alm_{15.7}Grs_{0.6}Adr_{4.3}Sps_{0.7}Uvr_{6.1},^d Prp_{72.6}Alm_{16.0}Grs_{1.9}Adr_{4.2}Sps_{0.6}Uvr_{4.7},^e Prp_{70.4}Alm_{16.0}Grs_{1.8}Adr_{2.1}Sps_{0.9}Uvr_{8.8},^f Prp_{72.6}Alm_{15.7}Grs_{0.6}Adr_{4.3}Sps_{0.7}Uvr_{6.1},^g Prp₆₈Alm₂₄Grs₅Sps₁;^g - refit the literature data by this study;^h - Hydrous sample

Prp - pyrope; Alm - Almandine; Grs - grossular; Sps - spessartine; Uvr - uvarovite; Adr - andradite; BLS = Brillouin light scattering; UI = ultrasonic interferometry; RPR = rectangular parallelepiped resonance. - means unavailable

Table S5. Elastic parameters of minerals used for density and velocity calculations

Formula	ρ (g/cm ³)	K_{S0} (GPa)	$(\partial K_S/\partial P)_T$	$(\partial^2 K_S/\partial P^2)_T$	$\partial K_S/\partial T$ (GPaK ⁻¹)	G_0 (GPa)	$(\partial G/\partial P)_T$	$(\partial^2 G/\partial P^2)_T$	$\partial G/\partial T$ (GPaK ⁻¹)	γ	α (10 ⁻⁵ K ⁻¹)	θ_E (K)	References
Prp ₁₀₀ (Mg ₃ Al ₂ Si ₃ O ₁₂)	3.565(3)	171(1)	4.3(2)	-	-0.016(1)	92.3(9)	1.5(1)	-	-0.0092(7)	1.15	2.543(5)	320	1
Alm ₁₀₀ (Fe ₃ Al ₂ Si ₃ O ₁₂)	4.3188(2)	174(1)	4.6(1)	-	-0.0267(7)	94.9(7)	1.06(6)	-	-0.0131(8)	1.22	1.85(1)	600	2
Grs ₁₀₀ (Ca ₃ Al ₂ Si ₃ O ₁₂)	3.5949(1)	168.4(7)	4.9(1)	-	-0.0136(5)	108.9(4)	1.39(4)	-	-0.0128(2)	1.22	2.09(2)	512	3
Uvr ₁₀₀ (Ca ₃ Cr ₂ Si ₃ O ₁₂)	3.8302(7)	162(2)	4.7(9)	-	-0.012(3)	92(1)	1.8(5)	-	-0.0128(2)	1.22	1.64(14)	473	4
Knr ₁₀₀ (Mg ₃ Cr ₂ Si ₃ O ₁₂)	3.8930(8)	160(2)	4.6(9)	-	-0.012(3)	92(1)	1.8(5)	-	-0.0128(2)	1.34	2.89(6)	477	5
Fo ₁₀₀ (Mg ₂ SiO ₄)	3.2214(2)	129.8(9)	4.45(5)	-	-0.018(2)	77.8(5)	1.8(1)	-0.10(2)	-0.013(1)	1.14	2.666(9)	484	6
Fa ₁₀₀ (Fe ₂ SiO ₄)	4.4020(7)	129.8(9)	4.45(5)	-	-0.018(2)	77.8(5)	1.8(1)	-0.10(2)	-0.013(1)	1.14	2.666(9)	484	7
En ₁₀₀ (Mg ₂ Si ₂ O ₆)	3.2039(2)	113(1)	8.8(1)	-0.68(6)	-0.0263(3)	75.9(7)	2.9(1)	-0.40(2)	-0.0136(3)	0.88	2.591(18)	510	8
Fs ₁₀₀ (Fe ₂ Si ₂ O ₆)	3.9985(3)	113(1)	8.8(1)	-0.68(6)	-0.0263(3)	75.9(7)	2.9(1)	-0.40(2)	-0.0136(3)	0.89	2.591(18)	510	9
MgTs ₁₀₀ (MgAlSiAlO ₆)	3.4153(5)	113(1)	8.8(1)	-0.68(6)	-0.0263(3)	75.9(7)	2.9(1)	-0.40(2)	-0.0136(3)	0.88	2.591(18)	510	10
CrEn ₁₀₀ (MgCrAlSiO ₆)	3.679(2)	113(1)	8.8(1)	-0.68(6)	-0.0263(3)	75.9(7)	2.9(1)	-0.40(2)	-0.0136(3)	0.88	2.591(18)	510	11
Jd ₁₀₀ (NaAlSi ₂ O ₆)	3.3287(7)	138(3)	3.9(1)	-	-0.012(1)	84(2)	1.09(4)	-	-0.011(1)	1.06	2.67(7)	343	12
Di ₁₀₀ (CaMgSi ₂ O ₆)	3.2787(4)	114.6(7)	5.4(4)	-0.2(1)	-0.012(1)	72.7(4)	1.9(2)	-0.07(4)	-0.011(1)	1.1	2.67(7)	343	13
Hd ₁₀₀ (CaFeSi ₂ O ₆)	3.6625(6)	116.6(8)	5.0(2)	-0.12(4)	-0.012(1)	69.8(7)	1.72(9)	-0.05(2)	-0.011(1)	1.1	2.67(7)	343	14
Kos ₁₀₀ (NaCrSi ₂ O ₆)	3.592(2)	138(3)	3.9(1)	-	-0.012(1)	84(2)	1.09(4)	-	-0.011(1)	1.06	2.67(7)	343	15
Cen ₁₀₀ (Mg ₂ Si ₂ O ₆)	3.2077(6)	114.6(7)	5.4(4)	-0.2(1)	-0.012(1)	72.7(4)	1.9(2)	-0.07(4)	-0.011(1)	1.1	2.67(7)	343	16
CaTs ₁₀₀ (CaAl ₂ SiO ₆)	3.45	114.6(7)	5.4(4)	-0.2(1)	-0.012(1)	72.7(4)	1.9(2)	-0.07(4)	-0.011(1)	1.1	2.67(7)	343	17

Note: Due to the lack of end-member elastic parameters, $\partial K_S/\partial T$ of Uvr₁₀₀ is converted from $\partial K_T/\partial T$ obtained from Gréaux & Yamada (2019); $\partial G/\partial T$ of Uvr₁₀₀ is assumed to be equal to that of Grs₁₀₀; G_0 , $(\partial G/\partial P)_T$ and $\partial G/\partial T$ of Knr₁₀₀ are assumed to be equal to that of Uvr₁₀₀, while $\partial K_S/\partial T$ and K_{S0} of Knr₁₀₀ are converted from $\partial K_T/\partial T$ and K_{T0} , respectively; the elastic parameters except density of San Carlos olivine (Angel et al., 2018; Mao et al., 2015; Zhang & Bass, 2016b) are used For Fo₁₀₀ and Fa₁₀₀; the elastic parameters K_{S0} , $(\partial K_S/\partial P)_T$, $(\partial^2 K_S/\partial P^2)_T$, G_0 (GPa), $(\partial G/\partial P)_T$, and $(\partial^2 G/\partial P^2)_T$ of San Carlos orthopyroxene (Zhang & Bass, 2016a), $\partial K_S/\partial T$ and $\partial G/\partial T$ of En₁₀₀ (Jackson et al., 2007), α of Ca-, Fe-, Al-bearing orthopyroxene (Faccincani et al., 2021) are used for En₁₀₀, Fs₁₀₀, CrEn₁₀₀ and MgTs₁₀₀; γ of En₁₀₀ is used For En₁₀₀, CrEn₁₀₀ and MgTs₁₀₀; the density of MgTs₁₀₀ is Calculated using a linear interpolation of the densities of En₁₀₀, Fs₁₀₀ and synthetic MgTs-rich orthopyroxene (Xu et al., 2020; Xu et al., 2022), while the density of CrEn is calculated using ρ (CrEn₁₀₀) = ρ (Kos₁₀₀) + ρ (MgTs₁₀₀) - ρ (Jd₁₀₀); the elastic parameters K_{S0} , $(\partial K_S/\partial P)_T$, $(\partial^2 K_S/\partial P^2)_T$, G_0 (GPa), $(\partial G/\partial P)_T$, $(\partial^2 G/\partial P^2)_T$, $\partial K_S/\partial T$, $\partial G/\partial T$ and γ of diopside (Jeanloz & Thompson, 1983; Li & Neuvill, 2010; Sang & Bass, 2014; Zhao et al., 1998) are used For Di₁₀₀, Cen₁₀₀ and CaTs₁₀₀; the elastic parameters K_{S0} , $(\partial K_S/\partial P)_T$, G_0 (GPa), $(\partial G/\partial P)_T$ and γ of Jadeite (Hao et al., 2020), $\partial K_S/\partial T$ and $\partial G/\partial T$ of diopside (Li & Neuvill, 2010) are used For Jd₁₀₀ and Kos₁₀₀; the elastic parameters K_{S0} , $(\partial K_S/\partial P)_T$, $(\partial^2 K_S/\partial P^2)_T$, G_0 (GPa), $(\partial G/\partial P)_T$, $(\partial^2 G/\partial P^2)_T$ of Fe-rich diopside (Fan et al., 2020), $\partial K_S/\partial T$, $\partial G/\partial T$ and γ of diopside are used For Hd₁₀₀. α of clinopyroxene (Faccincani et al., 2021) is used For All end-member clinopyroxenes. Fo-Forsterite; Fa-fayalite; En-enstatite; Fs-Ferrosilite; MgTs-Mg-tschermakite; Di-diopside; Jd-jadeite; Kos-kosmochlor; CrEn-Cr-enstatite; Hd-hedenbergite; Cen-clinoenstatite; CaTs-Ca-tschermakite; Prp-pyrope; Alm-Almandine; Grs-grossular; Uvr-uvarovite; Knr-knorringite. - means unavailable.

References: 1-(Chantel et al., 2016; Gwanmesia et al., 2006; Milani et al., 2015; Sinogeikin & Bass, 2000; Sinogeikin & Bass, 2002; Zhang et al., 1998; Zou, Gréaux, et al., 2012); 2-(Arimoto et al., 2015; Milani et al., 2015; Soga, 1967); 3-(Bass, 1989; Gwanmesia et al., 2014; Isaak et al., 1992; Milani et al., 2017); 4-(Bass, 1986; Gréaux & Yamada, 2019; Klemme et al., 2005; Wang & Ji, 2001); 5-(Bass, 1986; Dymshits et al., 2014; Gréaux & Yamada, 2019; Klemme et al., 2005; Wang & Ji, 2001); 6-(Angel et al., 2018; Kroll et al., 2012; Mao et al., 2015; Zhang & Bass, 2016b); 7-(Angel et al., 2018; Kroll et al., 2012; Mao et al., 2015; Zhang & Bass, 2016b); 8-(Faccincani et al., 2021; Jackson et al., 2007; Xu et al., 2018; Yang & Ghose, 1994; Zhang & Bass, 2016a); 9-(Faccincani et al., 2021; Hugh-Jones, 1997; Jackson et al., 2007; Xu et al., 2020; Yang & Ghose, 1994; Zhang & Bass, 2016a); 10-(Faccincani et al., 2021; Jackson et al., 2007; Xu et al., 2022; Yang & Ghose, 1994; Zhang & Bass, 2016a); 11-(Faccincani et al., 2021; Jackson et al., 2007; Ohashi, 1984; Yang & Ghose, 1994; Zhang & Bass, 2016a); 12-(Hao et al., 2020; Li & Neuvill, 2010; Zhao et al., 1997); 13-(Jeanloz & Thompson, 1983; Li & Neuvill, 2010; Sang & Bass, 2014; Zhao et al., 1998); 14-(Fan et al., 2020; Jeanloz & Thompson, 1983; Li & Neuvill, 2010; Tribaudino et al., 2008); 15-(Cameron et al., 1973; Hao et al., 2020; Li & Neuvill, 2010); 16-(Hugh-Jones, 1997; Jacobsen et al., 2010; Jeanloz & Thompson, 1983; Li & Neuvill, 2010; Sang & Bass, 2014); 17-(Jeanloz & Thompson, 1983; Li & Neuvill, 2010; Ma et al., 2009; Sang & Bass, 2014; Zhao et al., 1998)

References

- Angel, R.J., Alvaro, M., & Nestola, F. (2018). 40 years of mineral elasticity: a critical review and a new parameterisation of equations of state for mantle olivines and diamond inclusions. *Physics and Chemistry of Minerals*, 45(2), 95-113. <https://doi.org/10.1007/s00269-017-0900-7>
- Angel, R.J., Gonzalez-Platas, J., & Alvaro, M. (2014). EosFit7c and a Fortran module (library) for equation of state calculations. *Zeitschrift für Kristallographie - Crystalline Materials*, 229(5), 10.1515/zkri-2013-1711
- Arimoto, T., Gréaux, S., Irifune, T., Zhou, C., & Higo, Y. (2015). Sound velocities of Fe₃Al₂Si₃O₁₂ almandine up to 19 GPa and 1700 K. *Physics of the Earth and Planetary Interiors*, 246, 1-8. <https://doi.org/10.1016/j.pepi.2015.06.004>
- Babuška, V., Fiala, J., Kumazawa, M., Ohno, I., & Sumino, Y. (1978). Elastic properties of garnet solid-solution series. *Physics of the Earth and Planetary Interiors*, 16(2), 157-176. [https://doi.org/10.1016/0031-9201\(78\)90086-9](https://doi.org/10.1016/0031-9201(78)90086-9)
- Bass, J.D. (1986). Elasticity of uvarovite and andradite garnets. *Journal of Geophysical Research*, 91(B7), 7505-7516. <https://doi.org/10.1029/JB091iB07p07505>
- Bass, J.D. (1989). Elasticity of grossular and spessartite garnets by Brillouin spectroscopy. *Journal of Geophysical Research: Solid Earth*, 94(B6), 7621-7628. <https://doi.org/10.1029/JB094iB06p07621>
- Cameron, M., Sueno, S., Prewitt, C.T., & Papike, J.J. (1973). High-Temperature Crystal Chemistry of Acmite, Diopside, Hedenbergite, Jadeite, Spodumene, and Ureyite. *American Mineralogist*, 58, 594-618.
- Chantel, J., Manthilake, G.M., Frost, D.J., Beyer, C., Ballaran, T.B., Jing, Z., et al. (2016). Elastic wave velocities in polycrystalline Mg₃Al₂Si₃O₁₂-pyrope garnet to 24 GPa and 1300 K. *American Mineralogist*, 101(4), 991-997. <https://doi.org/10.2138/am-2016-5335>
- Chen, G., Cooke, J.A., Gwanmesia, G.D., & Liebermann, R.C. (1999). Elastic wave velocities of Mg₃Al₂Si₃O₁₂-pyrope garnet to 10 GPa. *American Mineralogist*, 84(3), 384-388. <https://doi.org/10.2138/am-1999-0322>
- Deen, T.J., Griffin, W., Begg, G., O'Reilly, S.Y., Natapov, L., & Hronsky, J. (2006). Thermal and compositional structure of the subcontinental lithospheric mantle: Derivation from shear wave seismic tomography. *Geochemistry, Geophysics, Geosystems*, 7(7), Q07003. <https://doi.org/10.1029/2005GC001120>
- Dymshits, A.M., Litasov, K.D., Sharygin, I.S., Shatskiy, A., Ohtani, E., Suzuki, A., et al. (2014). Thermal equation of state of majoritic khorringite and its significance for continental upper mantle. *Journal of Geophysical Research*, 119(11), 8034-8046. <https://doi.org/10.1002/2014JB011194>
- Faccincani, L., Faccini, B., Casetta, F., Mazzucchelli, M., Nestola, F., & Coltorti, M. (2021). EoS of mantle minerals coupled with composition and thermal state of the lithosphere: Inferring the density structure of peridotitic systems. *Lithos*, 404-405. 10.1016/j.lithos.2021.106483
- Fan, D., Fu, S., Lu, C., Xu, J., Zhang, Y., Tkachev, S.N., et al. (2020). Elasticity of single-crystal Fe-enriched diopside at high-pressure conditions: Implications for the origin of upper mantle low-velocity zones. *American Mineralogist: Journal of Earth and Planetary Materials*, 105(3), 363-374. <https://doi.org/10.2138/am-2020-7075>
- Fan, D., Xu, J., Lu, C., Tkachev, S.N., Li, B., Ye, Z., et al. (2019). Elasticity of single-crystal low water

- content hydrous pyrope at high-pressure and high-temperature conditions. *American Mineralogist*, 104(7), 1022-1031. <https://doi.org/10.2138/am-2019-6897>
- Gréaux, S., & Yamada, A. (2019). Density variations of Cr-rich garnets in the upper mantle inferred from the elasticity of uvarovite garnet. *Comptes Rendus Geoscience*, 351(2), 95-103. <https://doi.org/10.1016/j.crte.2018.09.012>
- Griffin, W., O'reilly, S.Y., Afonso, J.C., & Begg, G. (2009). The composition and evolution of lithospheric mantle: a re-evaluation and its tectonic implications. *Journal of Petrology*, 50(7), 1185-1204. <https://doi.org/10.1093/petrology/egn033>
- Gwanmesia, G., Jackson, I., & Liebermann, R. (2007). In search of the mixed derivative $\partial^2 M / \partial P \partial T$ (M = G, K): joint analysis of ultrasonic data for polycrystalline pyrope from gas-and solid-medium apparatus. *Physics and Chemistry of Minerals*, 34(2), 85-93.
- Gwanmesia, G.D., Wang, L., Heady, A., & Liebermann, R.C. (2014). Elasticity and sound velocities of polycrystalline grossular garnet (Ca₃Al₂Si₃O₁₂) at simultaneous high pressures and high temperatures. *Physics of the Earth and Planetary Interiors*, 228, 80-87. <https://doi.org/10.1016/j.pepi.2013.09.010>
- Gwanmesia, G.D., Zhang, J., Darling, K., Kung, J., Li, B., Wang, L., et al. (2006). Elasticity of polycrystalline pyrope (Mg₃Al₂Si₃O₁₂) to 9GPa and 1000°C. *Physics of the Earth and Planetary Interiors*, 155(3), 179-190. <https://doi.org/10.1016/j.pepi.2005.10.008>
- Hao, M., Zhang, J.S., Pierotti, C.E., Zhou, W.-Y., Zhang, D., & Dera, P. (2020). The seismically fastest chemical heterogeneity in the Earth's deep upper mantle—implications from the single-crystal thermoelastic properties of jadeite. *Earth and Planetary Science Letters*, 543, 116345. <https://doi.org/10.1016/j.epsl.2020.116345>
- Holland, T., & Powell, R. (2011). An improved and extended internally consistent thermodynamic dataset for phases of petrological interest, involving a new equation of state for solids. *Journal of Metamorphic Geology*, 29(3), 333-383. <https://doi.org/10.1111/j.1525-1314.2010.00923.x>
- Hugh-Jones, D. (1997). Thermal expansion of MgSiO₃ and FeSiO₃ ortho-and clinopyroxenes. *American Mineralogist*, 82(7-8), 689-696. <https://doi.org/10.2138/am-1997-7-806>
- Isaak, D.G., Anderson, O.L., & Oda, H. (1992). High-temperature thermal expansion and elasticity of calcium-rich garnets. *Physics and Chemistry of Minerals*, 19(2), 106-120. <https://doi.org/10.1007/BF00198608>
- Jackson, J.M., Sinogeikin, S.V., & Bass, J.D. (2007). Sound velocities and single-crystal elasticity of orthoenstatite to 1073 K at ambient pressure. *Physics of the Earth and Planetary Interiors*, 161(1-2), 1-12. <https://doi.org/10.1016/j.pepi.2006.11.002>
- Jacobsen, S.D., Liu, Z., Ballaran, T.B., Littlefield, E.F., Ehm, L., & Hemley, R.J. (2010). Effect of H₂O on upper mantle phase transitions in MgSiO₃: Is the depth of the seismic X-discontinuity an indicator of mantle water content? *Physics of the Earth and Planetary Interiors*, 183(1), 234-244. <https://doi.org/10.1016/j.pepi.2010.06.015>
- Jeanloz, R., & Thompson, A.B. (1983). Phase transitions and mantle discontinuities. *Reviews of Geophysics*, 21(1), 51-74. <https://doi.org/10.1029/RG021i001p00051>
- Klemme, S., Van Miltenburg, J., Javorsky, P., & Wastin, F. (2005). Thermodynamic properties of uvarovite garnet (Ca₃Cr₂Si₃O₁₂). *American Mineralogist*, 90(4), 663-666. <https://doi.org/10.2138/am.2005.1812>
- Kroll, H., Kirfel, A., Heinemann, R., & Barbier, B. (2012). Volume thermal expansion and related thermophysical parameters in the Mg,Fe olivine solid-solution series. *European Journal of*

- Mineralogy*, 24(6), 935-956. <https://doi.org/10.1127/0935-1221/2012/0024-2235>
- Leitner, B.J., Weidner, D.J., & Liebermann, R.C. (1980). Elasticity of single crystal pyrope and implications for garnet solid solution series. *Physics of the Earth and Planetary Interiors*, 22(2), 111-121. [https://doi.org/10.1016/0031-9201\(80\)90052-7](https://doi.org/10.1016/0031-9201(80)90052-7)
- Li, B., & Neuvill, D.R. (2010). Elasticity of diopside to 8GPa and 1073K and implications for the upper mantle. *Physics of the Earth and Planetary Interiors*, 183(3), 398-403. <https://doi.org/10.1016/j.pepi.2010.08.009>
- Ma, C., Simon, S.B., Rossman, G.R., & Grossman, L. (2009) End-member calcium Tschermak's pyroxene, CaAlAlSiO₆, from the Allende and Murray meteorites: occurrence, origin and significance.
- Mao, Z., Fan, D.W., Lin, J.F., Yang, J., Tkachev, S.N., Zhuravlev, K., et al. (2015). Elasticity of single-crystal olivine at high pressures and temperatures. *Earth and Planetary Science Letters*, 426, 204-215. <https://doi.org/10.1016/j.epsl.2015.06.045>
- Milani, S., Angel, R.J., Scandolo, L., Mazzucchelli, M.L., Ballaran, T.B., Klemme, S., et al. (2017). Thermo-elastic behavior of grossular garnet at high pressures and temperatures. *American Mineralogist*, 102(4), 851-859. <https://doi.org/10.2138/am-2017-5855>
- Milani, S., Nestola, F., Alvaro, M., Pasqual, D., Mazzucchelli, M.L., Domeneghetti, M.C., et al. (2015). Diamond–garnet geobarometry: The role of garnet compressibility and expansivity. *Lithos*, 227, 140-147. <https://doi.org/10.1016/j.lithos.2015.03.017>
- O'Neill, B., Bass, J.D., Rossman, G.R., Geiger, C.A., & Langer, K. (1991). Elastic properties of pyrope. *Physics and Chemistry of Minerals*, 17(7), 617-621. <https://doi.org/10.1007/BF00203841>
- Ohashi, Y. (1984). Polysynthetically-twinned structures of enstatite and wollastonite. *Physics and Chemistry of Minerals*, 10(5), 217-229. <https://doi.org/10.1007/BF00309314>
- Sang, L., & Bass, J.D. (2014). Single-crystal elasticity of diopside to 14 GPa by Brillouin scattering. *Physics of the Earth and Planetary Interiors*, 228, 75-79. <https://doi.org/10.1016/j.pepi.2013.12.011>
- Sinogeikin, S.V., & Bass, J.D. (2000). Single-crystal elasticity of pyrope and MgO to 20 GPa by Brillouin scattering in the diamond cell. *Physics of the Earth and Planetary Interiors*, 120(1), 43-62. [https://doi.org/10.1016/S0031-9201\(00\)00143-6](https://doi.org/10.1016/S0031-9201(00)00143-6)
- Sinogeikin, S.V., & Bass, J.D. (2002). Elasticity of pyrope and majorite–pyrope solid solutions to high temperatures. *Earth and Planetary Science Letters*, 203(1), 549-555. [https://doi.org/10.1016/S0012-821X\(02\)00851-8](https://doi.org/10.1016/S0012-821X(02)00851-8)
- Soga, N. (1967). Elastic constants of garnet under pressure and temperature. *Journal of Geophysical Research*, 72(16), 4227-4234. <https://doi.org/10.1029/JZ072i016p04227>
- Suzuki, I., & Anderson, O.L. (1983). Elasticity and thermal expansion of a natural garnet up to 1,000 K. *Journal of Physics of the Earth*, 31(2), 125-138. <https://doi.org/10.4294/jpe1952.31.125>
- Tribaudino, M., Nestola, F., Bruno, M., Ballaran, T.B., & Liebske, C. (2008). Thermal expansion along the NaAlSi₂O₆-NaFe³⁺Si₂O₆ and NaAlSi₂O₆-CaFe²⁺Si₂O₆ solid solutions. *Physics and Chemistry of Minerals*, 35(5), 241-248. <https://doi.org/10.1007/s00269-008-0217-7>
- Wang, Z., & Ji, S. (2001). Elasticity of six polycrystalline silicate garnets at pressure up to 3.0 GPa. *American Mineralogist*, 86(10), 1209-1218. <https://doi.org/10.2138/am-2001-1009>
- Xu, J., Fan, D., Zhang, D., Guo, X., Zhou, W., & Dera, P.K. (2020). Phase Transition of Enstatite-Ferrosilite Solid Solutions at High Pressure and High Temperature: Constraints on Metastable Orthopyroxene in Cold Subduction. *Geophysical Research Letters*, 47(12), e2020GL087363.

- <https://doi.org/10.1029/2020GL087363>
- Xu, J., Fan, D., Zhang, D., Ma, M., Zhou, Y., Tkachev, S.N., et al. (2022). Phase Transitions of Fe-, Al- and Ca-Bearing Orthopyroxenes at High Pressure and High Temperature: Implications for Metastable Orthopyroxenes in Stagnant Slabs. *Journal of Geophysical Research: Solid Earth*, 127(1), e2021JB023133. <https://doi.org/10.1029/2021JB023133>
- Xu, J., Zhang, D., Fan, D., Zhang, J.S., Hu, Y., Guo, X., et al. (2018). Phase Transitions in Orthoenstatite and Subduction Zone Dynamics: Effects of Water and Transition Metal Ions. *Journal of Geophysical Research: Solid Earth*, 123(4), 2723-2737. <https://doi.org/10.1002/2017JB015169>
- Yang, H., & Ghose, S. (1994). Thermal expansion, Debye temperature and Grüneisen parameter of synthetic (Fe, Mg)SiO₃ orthopyroxenes. *Physics and Chemistry of Minerals*, 20(8), 575-586. <https://doi.org/10.1007/BF00211853>
- Zhang, J.S., & Bass, J.D. (2016a). Single Crystal Elasticity of Natural Fe-bearing Orthoenstatite Across a High-Pressure Phase Transition. *Geophysical Research Letters*, 43(16), 8473-8481. <https://doi.org/10.1002/2016GL069963>
- Zhang, J.S., & Bass, J.D. (2016b). Sound velocities of olivine at high pressures and temperatures and the composition of Earth's upper mantle. *Geophysical Research Letters*, 43(18), 9611-9618. <https://doi.org/10.1002/2016GL069949>
- Zhang, L., Ahsbahs, H., & Kutoglu, A. (1998). Hydrostatic compression and crystal structure of pyrope to 33 GPa. *Physics and Chemistry of Minerals*, 25(4), 301-307. <https://doi.org/10.1007/s002690050118>
- Zhao, Y., Dreele, R.V., Zhang, J., & Weidner, D. (1998). Thermoelastic Equation of State of Monoclinic Pyroxene: CaMgSi₂O₆ Diopside. *The Review of High Pressure Science and Technology*, 7, 25-27. <https://doi.org/10.4131/jshpreview.7.25>
- Zhao, Y., Von Dreele, R.B., Shankland, T.J., Weidner, D.J., Zhang, J., Wang, Y., et al. (1997). Thermoelastic equation of state of jadeite NaAlSi₂O₆: An energy-dispersive Reitveld Refinement Study of low symmetry and multiple phases diffraction. *Geophysical Research Letters*, 24(1), 5-8. <https://doi.org/10.1029/96GL03769>
- Zou, Y., Gréaux, S., Irifune, T., Whitaker, M.L., Shinmei, T., & Higo, Y. (2012). Thermal equation of state of Mg₃Al₂Si₃O₁₂ pyrope garnet up to 19 GPa and 1,700 K. *Physics and Chemistry of Minerals*, 39(7), 589-598. <https://doi.org/10.1007/s00269-012-0514-z>
- Zou, Y., Irifune, T., Gréaux, S., Whitaker, M.L., Shinmei, T., Ohfuji, H., et al. (2012). Elasticity and sound velocities of polycrystalline Mg₃Al₂(SiO₄)₃ garnet up to 20 GPa and 1700 K. *Journal of Applied Physics*, 112(1), 014910. <https://doi.org/10.1063/1.4736407>